

Performance Impact of Idle Mode Capability on Dense Small Cell Networks with LoS and NLoS Transmissions

Ming Ding[‡], David López Pérez[†], Guoqiang Mao^{‡†□§♣}, Zihuai Lin[¶]

[‡]*Data61, Australia*

[†]*Nokia Bell Labs, Ireland*

[‡]*School of Computing and Communication, University of Technology Sydney, Australia*

[□]*School of Electronic Information & Communications, Huazhong University of Science & Technology, Wuhan, China*

[§]*School of Information and Commun. Engineering, Beijing University of Posts and Telecommunications, Beijing, China*

[¶]*The University of Sydney, Australia*

Abstract

In dense small cell networks (SCNs), a large number of base stations (BSs) can be put to idle modes without signal transmission, if there is no active user equipment (UE) within their coverage areas. Setting those BSs to idle modes can mitigate unnecessary inter-cell interference and reduce energy consumption. Such idle mode feature at BSs is referred to as the idle mode capability (IMC) and it can largely improve the performance of the 5th-generation (5G) networks. In this paper, we study the performance impact of the BS IMC on dense SCNs. Different from existing work, we consider a sophisticated and more realistic path loss model incorporating both line-of-sight (LoS) and non-line-of-sight (NLoS) transmissions. Analytical results are obtained for the coverage probability, the area spectral efficiency and the energy efficiency performance for SCNs with the BS IMC. An upper bound, a lower bound and an approximate expression of the density of the non-idle BSs are also derived. The performance impact of the IMC on network densification is shown to be significant. As the BS density surpasses the UE density, thus creating a surplus of BSs, the coverage probability will continuously increase toward one, which addresses the critical issue of coverage

probability decrease caused by the LoS/NLoS transmissions. The results derived from our analysis shed valuable new light on the deployment and the operation of future dense SCNs in 5G.

Index Terms

Stochastic geometry, Line-of-sight (LoS), Non-line-of-sight (NLoS), Dense small cell networks (SCNs), Coverage probability, Area spectral efficiency, Energy efficiency.

I. INTRODUCTION

Dense small cell networks (SCNs), comprising of remote radio heads, metrocells, picocells, femtocells, relay nodes, etc., have attracted significant attention as one of the most promising approaches to rapidly increase network capacity and meet the ever-increasing data traffic demands [1]. Indeed, the orthogonal deployment of dense SCNs within the existing macrocell networks [2], i.e., small cells and macrocells operating on different frequency spectrum (Small Cell Scenario #2a [2]), has been selected as the workhorse for capacity enhancement in the 4th-generation (4G) and the 5th-generation (5G) networks, developed by the 3rd Generation Partnership Project (3GPP) [3]. In this paper, we focus on the analysis of these dense SCNs with an orthogonal deployment in the existing macrocell networks.

In the seminal work of Andrews, Baccelli, and Ganti [4], a conclusion was reached that the density of base stations (BSs) would not affect the coverage probability performance in interference-limited¹ and fully-loaded² wireless networks, where the coverage probability is defined as the probability that the signal-to-interference-plus-noise ratio (SINR) of a typical user equipment (UE) is above a SINR threshold γ . Consequently, the area spectral efficiency (ASE) performance in bps/Hz/km² would scale linearly with the network densification [4]. The intuition of such conclusion is that the increase in the interference power caused by a denser network would be exactly compensated by the increase in the signal power due to the reduced distance between transmitters and receivers. This coverage probability behavior predicted in [4] is shown in Fig. 1.

¹In a interference-limited network, the power of each BS is set to a value much larger than the noise power.

²In a fully-loaded network, all BSs are active. Such assumption implies that the user density is infinity or much larger than the BS density. According to the results in [5], the user density should be at least 10 times higher than the BS density to make sure that almost all BSs are active.

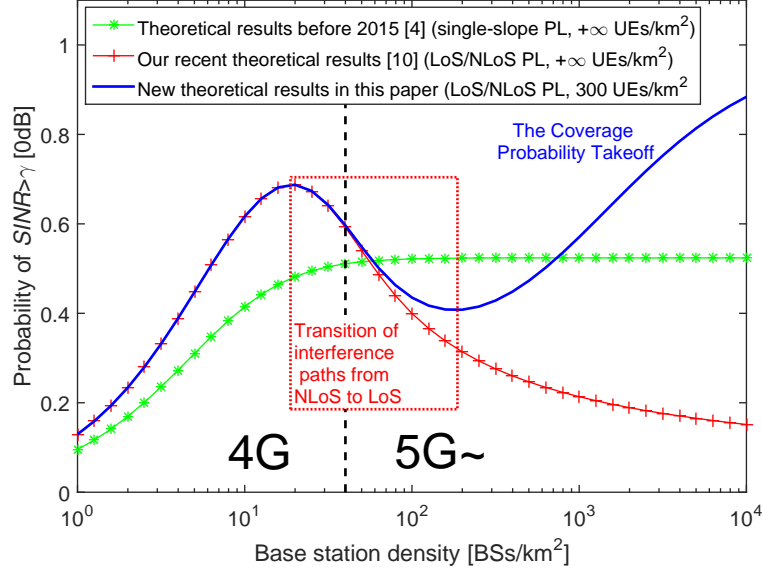


Fig. 1. Theoretical performance comparison of the coverage probability when the SINR threshold $\gamma = 0$ dB. Note that all the results are obtained using practical 3GPP channel models [6], [7], which will be introduced in details later. Moreover, the BS density regions for the 4G and 5G networks have been illustrated in the figure, considering that the typical BS density of the 4G SCNs is in the order of tens of BSs/km² [2], [3].

However, it is important to note that such conclusion was obtained with considerable simplifications on the network condition and propagation environment. For example, all BSs were assumed to be active and a single-slope path loss model was used. It would be interesting to investigate whether the conclusion still holds in real-world environment featuring more complicated BS behaviors and radio propagation environment. To this end, a few noteworthy studies have been carried out recently to revisit the network performance analysis of dense SCNs using more practical propagation models. In [8], the authors considered a multi-slope piece-wise path loss function, while in [9], the authors modeled line-of-sight (LoS) and non-line-of-sight (NLoS) transmissions as probabilistic events for a millimeter wave communication scenario. In our recent work [10], [11], we further considered both piece-wise path loss functions and probabilistic LoS and NLoS transmissions. Our analysis demonstrated that when the BS density is larger than a threshold λ^* , the coverage probability performance will decrease as the SCN becomes denser, which in turn may make the ASE suffer from a slow growth or even a *decrease* as the BS density increases. The intuition behind this result is that the interference power increases faster than the signal power due to the transition of a large number of interference paths from NLoS to LoS with the network densification. Fig. 1 shows this coverage probability result, where λ^* is around 20 BSs/km². The key message is

that, when deploying dense SCNs, it should not be taken for granted that an increased BS density will always lead to improved network performance. Indeed, the opposite case may happen.

Another important factor that needs to be taken into account in dense SCN performance analysis is that as the BS density increases, the number of BSs being muted will also increase. More specifically, since the UE density is finite in practical networks, a large number of BSs can turn off their transmission modules in dense SCNs, if there is no active UE within their coverage areas. Setting those BSs to idle modes can mitigate unnecessary inter-cell interference and reduce energy consumption [5], [12]–[14]. In other words, by dynamically muting idle BSs, the interference suffered by UEs from always-on control channels, e.g., synchronization and broadcast channels, and data channels can be reduced, thus improving UEs' coverage probability. This idle mode feature at BSs is referred to as the idle mode capability (IMC) hereafter.

Furthermore, the energy efficiency (EE) of SCNs with the IMC can be significantly enhanced because (i) BSs without any active UE can be temporarily put into an idle mode with low energy consumption, and (ii) every active BS usually benefits from high-SINR and thus energy-efficient links with its associated UEs due to the BS diversity gain [5], i.e., each UE selects its serving BS with the highest SINR from a surplus of BSs in dense SCNs. It is very important to note that a BS in an idle mode may still consume a non-negligible amount of energy, thus impacting the EE of SCNs. In this paper, we use a practical power model developed in the Green-Touch project [15] to evaluate the EE performance. Such power model will be formally introduced later.

In this paper, we investigate for the first time the performance impact of the IMC on dense SCNs considering LoS and NLoS transmissions. As an example to demonstrate such impact, our results with a UE density of 300 UEs/km² (a typical UE density in 5G [3]) are compared with the existing results [4], [10] in Fig. 1. The performance impact of the IMC on the coverage probability is shown to be significant. As the BS density surpasses the UE density in future dense and ultra-dense SCNs [3], thus creating a surplus of BSs, the coverage probability will continuously increase toward one, addressing the critical issue of coverage probability decrease caused by the NLoS to LoS transition of interference paths shown in

Fig. 1. Such performance behavior of the coverage probability increasing toward one in dense SCNs, is referred to as *the Coverage Probability Takeoff* hereafter. The intuition behind *the Coverage Probability Takeoff* is that beyond a certain BS density threshold, the interference power will basically remain constant with the network densification due to the IMC at BSs, while the signal power will continuously rise due to the BS diversity gain, thus leading to a better SINR performance as the network evolves into a dense SCN.

Compared with existing work, the main contributions of this paper are:

- Analytical results are obtained for the coverage probability and the ASE performance of SCNs with the IMC at BSs using a general path loss model incorporating both LoS and NLoS transmissions. Note that existing work on the IMC only treated a single-slope path loss model, where a UE is always associated with its nearest BS [5], [13], while our work considers more practical path loss models with probabilistic LoS and NLoS transmissions, where UEs may connect to a farther BS with a LoS path.
- An upper bound, a lower bound and an approximate expression of the density of the active BSs are derived for SCNs with the IMC, considering practical path loss models with probabilistic LoS and NLoS transmissions.
- The performance improvement in terms of the EE is also investigated for dense SCNs using practical energy models developed in the Green-Touch project [15]. In particular, for practical power models and 3GPP path loss functions, our studies reveal that compared with the baseline scheme with all BSs active, various IMC modes can double or even triple the EE performance in dense SCNs, e.g., when the BS density is 10^3 BSs/km².

The rest of this paper is structured as follows. Section II provides a brief review of related work. Section III describes the system model featuring the IMC at BSs. Section IV presents our theoretical results on the coverage probability, the ASE, the density of the active BSs and the EE performance, with applications in 3GPP special cases. The numerical results are discussed in Section V, with remarks shedding new light on the performance and the deployment of future dense SCNs with the IMC. Finally, the conclusions are drawn in Section VI.

II. RELATED WORK

In stochastic geometry, BS positions are typically modeled as a Homogeneous Poisson Point Process (HPPP) on the plane, and closed-form expressions of the coverage probability performance is then investigated for some scenarios in single-tier cellular networks [4] and multi-tier cellular networks [16]. The major conclusion in [4], [16] is that neither the number of cells nor the number of cell tiers changes the coverage probability in interference-limited and fully-loaded wireless networks.

Recently, a few noteworthy studies have been carried out to further investigate the network performance analysis for dense and ultra-dense SCNs under more practical propagation models. As discussed in Section I, the authors of [8] and [9] found that the coverage probability performance will start to decrease when the BS density is sufficiently large, but such decrease of coverage probability does *not* change the monotonic increase of the ASE as the BS density increases.

In our recent work [10] considering the impact of probabilistic LoS and NLoS transmissions, we presented a new finding that the coverage probability performance will initially increase with the increase of the BS density, but when the BS density is larger than a threshold λ^* , the coverage probability performance will decrease as the SCN becomes denser, which in turn may make the ASE suffer from a slow growth or even a *decrease* as the BS density further increases. Such result was not only quantitatively but also qualitatively different from previous results in [4], [8], [9]. The intuition behind this result is that as the BS density becomes larger than a threshold, the interference power increases faster than the signal power due to the transition of a large number of interference paths from NLoS to LoS. Our analysis also demonstrated that such decrease of the coverage probability gradually slows down as the SCN becomes ultra-dense. This is because at a very high BS density, both the signal power and the interference power at the typical UE become LoS dominated, and thus their ratio reaches a statistically stable level.

All of the above work did not consider an important factor that as the BS density increases, a large number of BSs can be put to idle modes without signal transmission, if there is no active UE within their coverage areas. This is a new network behavior arising from dense

SCNs and a limited number of active UEs, i.e., it may happen that a significant number of BSs may not have any active UE in their coverage areas during certain time periods. Therefore, such BSs should mute their transmission to mitigate unnecessary inter-cell interference and reduce energy consumption [5], [12]–[14]. Up to now, the limited existing work that did consider the IMC, only treated a simplistic single-slope path loss model for homogeneous SCNs [5], [12]–[14] or for the co-channel deployment of heterogeneous networks [14]. Such path loss assumption might not be practical for realistic SCNs. As revealed in our earlier work [10], [11], when more realistic and complicated propagation models such as those considering LoS and NLoS transmissions, are used, the performance of dense SCN may significantly differ from that assuming a simplistic single-slope path loss model. Motivated by the above observations, in this paper, we investigate for the first time the performance impact of *the IMC* on dense SCNs considering probabilistic *LoS and NLoS transmissions*.

III. SYSTEM MODEL

We consider a downlink (DL) cellular network with BSs deployed on a plane according to a homogeneous Poisson point process (HPPP) Φ with a density of λ BSs/km². Active UEs are Poisson distributed in the considered DL network with a density of ρ UEs/km². Here, we only consider active UEs in the network because non-active UEs do not trigger DL data transmission, and thus they are ignored in our analysis. Note that the total UE number in cellular networks should be much higher the number of the active UEs, but at a certain time slot and on a certain frequency band, the active UEs with data traffic demands are not too many. As discussed in Section I, A typical density of the active UEs in 5G is round 300 UEs/km² [3].

In our previous work [10], [11] and other related work [8], [9], ρ was assumed to be infinite or considerably larger than λ so that each BS has at least one associated UE in its coverage. In this work, we impose no such constraint on ρ , and hence a BS with the IMC will enter idle modes if there is no UE connected to it, which reduces interference to neighboring UEs as well as energy consumption. Since UEs are randomly and uniformly distributed in the network, we adopt a common assumption that the active BSs also follow an HPPP distribution $\tilde{\Phi}$ [5], the density of which is denoted by $\tilde{\lambda}$ BSs/km². Note that $0 \leq \tilde{\lambda} \leq \lambda$,

and a larger ρ requires more active BSs with a larger $\tilde{\lambda}$ to serve the active UEs.

Following [10], [11], we adopt a very general path loss model, in which the path loss $\zeta(r)$ as a function of r is segmented into N pieces written as

$$\zeta(r) = \begin{cases} \zeta_1(r), & \text{when } 0 \leq r \leq d_1 \\ \zeta_2(r), & \text{when } d_1 < r \leq d_2 \\ \vdots & \vdots \\ \zeta_N(r), & \text{when } r > d_{N-1} \end{cases}, \quad (1)$$

where each piece $\zeta_n(r)$, $n \in \{1, 2, \dots, N\}$ is modeled as

$$\zeta_n(r) = \begin{cases} \zeta_n^L(r) = A_n^L r^{-\alpha_n^L}, & \text{LoS Probability: } \Pr_n^L(r) \\ \zeta_n^{NL}(r) = A_n^{NL} r^{-\alpha_n^{NL}}, & \text{NLoS Probability: } 1 - \Pr_n^L(r) \end{cases}, \quad (2)$$

where

- $\zeta_n^L(r)$ and $\zeta_n^{NL}(r)$, $n \in \{1, 2, \dots, N\}$ are the n -th piece path loss functions for the LoS transmission and the NLoS transmission, respectively
- A_n^L and A_n^{NL} are the path losses at a reference distance $r = 1$ for the LoS and the NLoS cases, respectively
- α_n^L and α_n^{NL} are the path loss exponents for the LoS and the NLoS cases, respectively

In practice, A_n^L , A_n^{NL} , α_n^L and α_n^{NL} are constants obtainable from field tests [6], [7]. Moreover, $\Pr_n^L(r)$ is the n -th piece LoS probability function that a transmitter and a receiver separated by a distance r has a LoS path, which is assumed to be *a monotonically decreasing function* with regard to r . Such assumption has been confirmed by existing measurement studies [6], [7]. For convenience, $\{\zeta_n^L(r)\}$ and $\{\zeta_n^{NL}(r)\}$ are further stacked into piece-wise functions written as

$$\zeta^{Path}(r) = \begin{cases} \zeta_1^{Path}(r), & \text{when } 0 \leq r \leq d_1 \\ \zeta_2^{Path}(r), & \text{when } d_1 < r \leq d_2 \\ \vdots & \vdots \\ \zeta_N^{Path}(r), & \text{when } r > d_{N-1} \end{cases}, \quad (3)$$

where the string variable $Path$ takes the value of “L” and “NL” for the LoS and the NLoS cases, respectively.

Besides, $\{\Pr_n^L(r)\}$ is stacked into a piece-wise function as

$$\Pr^L(r) = \begin{cases} \Pr_1^L(r), & \text{when } 0 \leq r \leq d_1 \\ \Pr_2^L(r), & \text{when } d_1 < r \leq d_2 \\ \vdots & \vdots \\ \Pr_N^L(r), & \text{when } r > d_{N-1} \end{cases}. \quad (4)$$

Note that the generality and the practicality of the adopted path loss model (1) have been well established in [10]. In more detail, this model is consistent with the ones adopted in the 3GPP [6], [7], and includes those models considered in [8] and [9] as its special cases. More specifically, in [8], only NLoS transmissions were considered, i.e., assuming $\Pr_n^L(r) = 0, \forall n \in \{1, 2, \dots, N\}$ in (1). In [9], only one piece of path loss function with one LoS path loss exponent and one NLoS path loss exponent was considered, i.e., assuming $N = 1$ in (1).

In this paper, we assume a practical user association strategy (UAS), in which each UE is connected to the BS with the smallest path loss (i.e., with the largest $\zeta(r)$) to the UE [9], [10]. Note that in our previous work [11] and some other existing work [4], [8], it was assumed that each UE should be associated with its closest BS. Such assumption is not appropriate for the considered path loss model in (1), because in practice a UE should connect to a BS offering the largest received signal strength. Such BS does not necessarily have to be the nearest one to the UE. It could be a farther one with a strong LoS path. Moreover, we assume that each BS/UE is equipped with an isotropic antenna, and that the multi-path fading between a BS and a UE is modeled as independently identical distributed (i.i.d.) Rayleigh fading [8]–[11]. Note that a more practical Rician fading will also be considered in Section V to show its minor impact on our conclusions.

IV. MAIN RESULTS

Using the theory of stochastic geometry, we study the performance of SCNs in terms of the coverage probability, the ASE and the EE by considering the performance of a typical

UE located at the origin o .

A. The Coverage Probability

First, we investigate the coverage probability that the typical UE's SINR is above a designated threshold γ :

$$p^{\text{cov}}(\lambda, \gamma) = \Pr[\text{SINR} > \gamma], \quad (5)$$

where the SINR is computed by

$$\text{SINR} = \frac{P\zeta(r)h}{I_{\text{agg}} + P_{\text{N}}}. \quad (6)$$

Here, h is the channel gain, which is modeled as an exponentially distributed random variable (RV) with a mean of one in accordance with our consideration of Rayleigh fading mentioned above, P and P_{N} are the BS transmission power and the additive white Gaussian noise (AWGN) power at each UE, respectively, and I_{agg} is the cumulative interference given by

$$I_{\text{agg}} = \sum_{i: b_i \in \tilde{\Phi} \setminus b_o} P\beta_i g_i, \quad (7)$$

where b_o is the BS at the origin and serves the typical UE located at distance r , and b_i , β_i and g_i are the i -th interfering BS, the path loss from b_i to the typical UE and the multi-path fading channel gain associated with b_i , respectively. Note that when all BSs are assumed to be active, the set of all BSs Φ should be used in the expression of I_{agg} [10], [11]. Here, in (7), only the active BSs in $\tilde{\Phi} \setminus b_o$ inject effective interference into the network, where $\tilde{\Phi}$ denotes the set of all active BSs, and the other BSs in idle modes are not taken into account in the analysis of I_{agg} .

Based on the path loss model in (1) and the adopted UAS, we present our result of $p^{\text{cov}}(\lambda, \gamma)$ in Theorem 1.

For Theorem 1, it is important to note that:

- The impact of the serving BS selection on the coverage probability is measured by (9) and (10), the expressions of which are thus based on λ , not on $\tilde{\lambda}$.
- The impact of I_{agg} on the coverage probability is measured by (14) and (16). Since only the active BSs emit effective interference into the considered SCN, the expressions of

Theorem 1. Considering the path loss model in (1) and the presented UAS, the probability of coverage $p^{\text{cov}}(\lambda, \gamma)$ can be derived as

$$p^{\text{cov}}(\lambda, \gamma) = \sum_{n=1}^N (T_n^{\text{L}} + T_n^{\text{NL}}), \quad (8)$$

where $T_n^{\text{L}} = \int_{d_{n-1}}^{d_n} \Pr \left[\frac{P\zeta_n^{\text{L}}(r)h}{I_{\text{agg}} + P_{\text{N}}} > \gamma \right] f_{R,n}^{\text{L}}(r) dr$, $T_n^{\text{NL}} = \int_{d_{n-1}}^{d_n} \Pr \left[\frac{P\zeta_n^{\text{NL}}(r)h}{I_{\text{agg}} + P_{\text{N}}} > \gamma \right] f_{R,n}^{\text{NL}}(r) dr$, and d_0 and d_N are defined as 0 and $+\infty$, respectively. Moreover, $f_{R,n}^{\text{L}}(r)$ and $f_{R,n}^{\text{NL}}(r)$ ($d_{n-1} < r \leq d_n$), are represented by

$$f_{R,n}^{\text{L}}(r) = \exp \left(- \int_0^{r_1} (1 - \Pr^{\text{L}}(u)) 2\pi u \lambda du \right) \exp \left(- \int_0^r \Pr^{\text{L}}(u) 2\pi u \lambda du \right) \Pr_n^{\text{L}}(r) 2\pi r \lambda, \quad (9)$$

and

$$f_{R,n}^{\text{NL}}(r) = \exp \left(- \int_0^{r_2} \Pr^{\text{L}}(u) 2\pi u \lambda du \right) \exp \left(- \int_0^r (1 - \Pr^{\text{L}}(u)) 2\pi u \lambda du \right) (1 - \Pr_n^{\text{L}}(r)) 2\pi r \lambda, \quad (10)$$

where r_1 and r_2 are given implicitly by the following equations as

$$r_1 = \arg \left\{ \zeta_n^{\text{NL}}(r_1) = \zeta_n^{\text{L}}(r) \right\}, \quad (11)$$

and

$$r_2 = \arg \left\{ \zeta^{\text{L}}(r_2) = \zeta_n^{\text{NL}}(r) \right\}. \quad (12)$$

In addition, $\Pr \left[\frac{P\zeta_n^{\text{L}}(r)h}{I_{\text{agg}} + P_{\text{N}}} > \gamma \right]$ and $\Pr \left[\frac{P\zeta_n^{\text{NL}}(r)h}{I_{\text{agg}} + P_{\text{N}}} > \gamma \right]$ are respectively computed by

$$\Pr \left[\frac{P\zeta_n^{\text{L}}(r)h}{I_{\text{agg}} + P_{\text{N}}} > \gamma \right] = \exp \left(- \frac{\gamma P_{\text{N}}}{P\zeta_n^{\text{L}}(r)} \right) \mathcal{L}_{I_{\text{agg}}}^{\text{L}} \left(\frac{\gamma}{P\zeta_n^{\text{L}}(r)} \right), \quad (13)$$

where $\mathcal{L}_{I_{\text{agg}}}^{\text{L}}(s)$ is the Laplace transform of I_{agg} for LoS signal transmission evaluated at s , which can be further written as

$$\mathcal{L}_{I_{\text{agg}}}^{\text{L}}(s) = \exp \left(-2\pi\tilde{\lambda} \int_r^{+\infty} \frac{\Pr^{\text{L}}(u)u}{1 + (sP\zeta^{\text{L}}(u))^{-1}} du \right) \exp \left(-2\pi\tilde{\lambda} \int_{r_1}^{+\infty} \frac{[1 - \Pr^{\text{L}}(u)]u}{1 + (sP\zeta^{\text{NL}}(u))^{-1}} du \right), \quad (14)$$

and

$$\Pr \left[\frac{P\zeta_n^{\text{NL}}(r)h}{I_{\text{agg}} + P_{\text{N}}} > \gamma \right] = \exp \left(- \frac{\gamma P_{\text{N}}}{P\zeta_n^{\text{NL}}(r)} \right) \mathcal{L}_{I_{\text{agg}}}^{\text{NL}} \left(\frac{\gamma}{P\zeta_n^{\text{NL}}(r)} \right), \quad (15)$$

where $\mathcal{L}_{I_{\text{agg}}}^{\text{NL}}(s)$ is the Laplace transform of I_{agg} for NLoS signal transmission evaluated at s , which can be further written as

$$\mathcal{L}_{I_{\text{agg}}}^{\text{NL}}(s) = \exp \left(-2\pi\tilde{\lambda} \int_{r_2}^{+\infty} \frac{\Pr^{\text{L}}(u)u}{1 + (sP\zeta^{\text{L}}(u))^{-1}} du \right) \exp \left(-2\pi\tilde{\lambda} \int_r^{+\infty} \frac{[1 - \Pr^{\text{L}}(u)]u}{1 + (sP\zeta^{\text{NL}}(u))^{-1}} du \right). \quad (16)$$

Proof: See Appendix A. ■

(14) and (16) are thus based on $\tilde{\lambda}$, not on λ .

- The derivation of $\tilde{\lambda}$ is non-trivial, and it will be treated later in the following subsections.

B. The Area Spectral Efficiency

Similar to [10], [11], we also investigate the area spectral efficiency (ASE) performance in bps/Hz/km², which is defined as

$$A^{\text{ASE}}(\lambda, \gamma_0) = \tilde{\lambda} \int_{\gamma_0}^{+\infty} \log_2(1 + \gamma) f_r(\lambda, \gamma) d\gamma, \quad (17)$$

where γ_0 is the minimum working SINR for the considered SCN, and $f_r(\lambda, \gamma)$ is the probability density function (PDF) of the SINR observed at the typical UE at a particular value of λ . It is important to note that:

- Unlike [10], [11], $\tilde{\lambda}$ is used in the expression of $A^{\text{ASE}}(\lambda, \gamma_0)$ because only the active BSs make an effective contribution to the ASE.
- The ASE defined in this paper is different from that in [8], where a constant rate based on γ_0 is assumed for the typical UE, no matter what the actual SINR value is. The definition of the ASE in (17) can better capture the dependence of the transmission rate on SINR, but it is less tractable to analyze, as it requires one more fold of numerical integral compared with [8].
- Regarding the computational complexity, in order to obtain $p^{\text{cov}}(\lambda, \gamma)$ presented in Theorem 1, for a general case, three folds of integrals are respectively required for the calculation of $\{f_{R,n}^{\text{Path}}(r)\}$, $\{\mathcal{L}_{I_{\text{agg}}}(\frac{\gamma}{P\zeta_n^{\text{Path}}(r)})\}$, and $\{T_n^{\text{Path}}\}$, where the string variable *Path* takes the value of “L” (for the LoS case) or “NL” (for the NLoS case). Note that an additional fold of integral is needed for the calculation of $A^{\text{ASE}}(\lambda, \gamma_0)$ in (17), making it a 4-fold integral computation.

Based on the definition of $p^{\text{cov}}(\lambda, \gamma)$ in (5), which is the complementary cumulative distribution function (CCDF) of SINR, $f_r(\lambda, \gamma)$ can be computed by

$$f_r(\lambda, \gamma) = \frac{\partial (1 - p^{\text{cov}}(\lambda, \gamma))}{\partial \gamma}. \quad (18)$$

From the results of $p^{\text{cov}}(\lambda, \gamma)$ and $A^{\text{ASE}}(\lambda, \gamma_0)$ respectively presented in (5) and (17), we can now analyze these two performance measures for the adopted UAS. The key step to do

so is to accurately derive $\tilde{\lambda}$, i.e., the density of the active BSs.

In [5], the authors derived an approximate expression of $\tilde{\lambda}$ based on the distribution of the Voronoi cell size assuming that each UE should be associated with *the nearest BS*. The main result in [5] is as follows,

$$\tilde{\lambda}^{\text{minDis}} \approx \lambda \left[1 - \frac{1}{\left(1 + \frac{\rho}{q\lambda}\right)^q} \right] \triangleq \lambda_0(q), \quad (19)$$

where $\tilde{\lambda}^{\text{minDis}}$ is the density of the active BSs under the assumption that each UE should connect to its nearest BS. An empirical value of 3.5 was suggested for q in [5]. The approximation was shown to be very accurate in existing work [5], [13], [14] assuming a nearest-distance UAS. In this work, a more realistic signal strength based UAS is adopted, and thus the corresponding result in [5] cannot be directly applied to Theorem 1. Instead, we need to derive $\tilde{\lambda}$ for the adopted UAS considering probabilistic LoS and NLoS transmissions. Our main results are presented in the following three subsections.

C. An Upper Bound of $\tilde{\lambda}$

First, we propose an upper bound of $\tilde{\lambda}$ in Theorem 2.

Theorem 2. *Based on the path loss model in (1) and the presented UAS, $\tilde{\lambda}$ can be upper bounded by*

$$\tilde{\lambda} \leq \lambda (1 - Q^{\text{off}}) \triangleq \tilde{\lambda}^{\text{UB}}, \quad (20)$$

where

$$Q^{\text{off}} = \lim_{r_{\text{max}} \rightarrow +\infty} \sum_{k=0}^{+\infty} \{\Pr[w \approx b]\}^k \frac{\lambda_{\Omega}^k e^{-\lambda_{\Omega}}}{k!}, \quad (21)$$

where $\lambda_{\Omega} = \rho\pi r_{\text{max}}^2$, and $\Pr[w \approx b]$ represents the probability that a UE w is not associated with BS b and it can be computed by

$$\Pr[w \approx b] = \int_0^{r_{\text{max}}} \Pr[w \approx b | r] \frac{2r}{r_{\text{max}}^2} dr, \quad (22)$$

and

$$\Pr[w \approx b | r] = [F_R^{\text{L}}(r) + F_R^{\text{NL}}(r_1)] \Pr^{\text{L}}(r) + [F_R^{\text{L}}(r_2) + F_R^{\text{NL}}(r)] [1 - \Pr^{\text{L}}(r)], \quad (23)$$

where $F_R^L(r) = \int_0^r f_R^L(u) du$, $F_R^{NL}(r) = \int_0^r f_R^{NL}(u) du$, and r_1 and r_2 are defined in (11) and (12), respectively.

Proof: See Appendix B. ■

D. A Lower Bound of $\tilde{\lambda}$

Next, we propose a lower bound of $\tilde{\lambda}$ in Theorem 3.

Theorem 3. *Based on the path loss model in (1) and the presented UAS, $\tilde{\lambda}$ can be lower bounded by*

$$\tilde{\lambda} \geq \tilde{\lambda}^{\min\text{Dis}} \triangleq \tilde{\lambda}^{\text{LB}}. \quad (24)$$

Proof: See Appendix C. ■

As discussed in Subsection IV-B, the exact expression of $\tilde{\lambda}^{\min\text{Dis}}$ is still unknown up to now, but it can be well approximated by $\lambda_0(q)$ shown in (19).

E. The Proposed Approximation of $\tilde{\lambda}$

Considering the lower bound of $\tilde{\lambda}$ derived in Theorem 3, and the fact that the approximate expression of such lower bound is *an increasing function* with respect to q , we propose Proposition 4 to obtain an approximate value of $\tilde{\lambda}$.

Proposition 4. *Based on the path loss model in (1) and the adopted UAS, we propose to approximate $\tilde{\lambda}$ by*

$$\tilde{\lambda} \approx \lambda_0(q^*), \quad (25)$$

where $3.5 \leq q^* \leq \arg \left\{ \lambda_0(x) = \tilde{\lambda}^{\text{UB}} \right\}_x$ and $\tilde{\lambda}^{\text{UB}}$ is computed from (20).

Note that the range of q^* in Proposition 4 is obtained according to the derived upper bound and lower bound of $\tilde{\lambda}$ presented in Theorem 2 and Theorem 3, respectively. Apparently, the value of q^* depends on the specific forms of the path loss model given by (3) and (4). Hence, q^* should be numerically found for specific path loss models in consideration. Fortunately, with the deterministic bounds of q^* characterized in Proposition 4, the value of q^* can be efficiently found using offline computation based on the bisection method [17] by minimizing

the difference between the approximate $\tilde{\lambda}$ in (25) and the simulation results of $\tilde{\lambda}$. Note that such difference should be accounted and averaged over all possible values of λ because $\lambda_0(q^*)$ also varies with λ . The average difference can be measured by, e.g., the mean squared error (MSE), giving rise to the numerical search of q^* based on the minimum MSE (MMSE) criterion.

F. The Energy Efficiency

Deploying dense SCNs poses some concerns in terms of energy consumption. Hence, the energy efficiency (EE) of dense SCNs should be carefully considered to allow for their sustainable deployments. When evaluating the BS energy consumption, it is very important to note that a BS in idle modes may still consume a non-negligible amount of energy, thus impacting the EE of SCNs. In this paper, we use a practical power model developed in the Green-Touch project [15]. This power model estimates the power consumption of a cellular BS, and is based on tailored modeling principles and scaling rules for each BS component i.e., power amplifier, analogue front-end, digital base band, digital control and backhaul interface and power supply. Moreover, it includes different optimized idle modes and provides a large flexibility, i.e., multiple BS types are available, which can be configured with multiple parameters, such as bandwidth, transmit power, number of antenna chains, system load, duplex mode, etc. Among the provided idle modes in the Green-Touch project, we consider *the Green-Touch slow idle mode* and *the Green-Touch shut-down mode*, where most components of an idle BS are deactivated. Note that these two modes are the most energy-efficient ones defined by the Green-Touch project.

Here, the total power of each idle SCN BS and that of each active SCN BS are respectively denoted by $P_{\text{IMC}}^{\text{TOT}}(\lambda)$ and $P_{\text{ACT}}^{\text{TOT}}(\lambda)$, then we can define the EE in the unit of bits/J for the entire SCN as

$$EE(\lambda, \gamma_0) = \frac{A^{\text{ASE}}(\lambda, \gamma_0) \times BW}{\tilde{\lambda} P_{\text{ACT}}^{\text{TOT}}(\lambda) + (\lambda - \tilde{\lambda}) P_{\text{IMC}}^{\text{TOT}}(\lambda)}, \quad (26)$$

where the area spectral efficiency $A^{\text{ASE}}(\lambda, \gamma_0)$ is obtained from (17) and BW denotes the system bandwidth in Hz. It is important to note that in practice $P_{\text{IMC}}^{\text{TOT}}(\lambda)$ and $P_{\text{ACT}}^{\text{TOT}}(\lambda)$ depend on the BS density λ because the BS transmission power decreases with the network

densification considering the interference limited SCNs [3]. Nevertheless, in previous subsections, we assume that the BS transmission power P is independent of λ in (6) because (i) it brings convenient expressions for our main results; and (ii) it has a minor impact on the ASE performance for dense SCNs, which will be verified in Section V.

Based on the definition of the EE given by (26), in Section V we will evaluate the impact of the network densification on $EE(\lambda, \gamma_0)$ with the practical Green-Touch power models and the 3GPP special cases of path loss functions, which will be introduced in the next subsection.

G. The 3GPP Special Cases

As a special case for our analytical results, following [10], we consider a two-piece path loss and a linear LoS probability functions defined by the 3GPP [6], [7]. Specifically, we use the path loss function $\zeta(r)$, defined in the 3GPP as [6]

$$\zeta(r) = \begin{cases} A^L r^{-\alpha^L}, & \text{LoS: } \Pr^L(r) \\ A^{NL} r^{-\alpha^{NL}}, & \text{NLoS: } 1 - \Pr^L(r) \end{cases}, \quad (27)$$

together with a linear LoS probability function of $\Pr^L(r)$, defined in the 3GPP as [7]

$$\Pr^L(r) = \begin{cases} 1 - \frac{r}{d_1}, & 0 < r \leq d_1 \\ 0, & r > d_1 \end{cases}, \quad (28)$$

where d_1 is a constant [7].

Considering the general path loss model presented in (1), the combined path loss model presented in (27) and (28) can be deemed as a special case of (1) with the following substitution: $N = 2$, $\zeta_1^L(r) = \zeta_2^L(r) = A^L r^{-\alpha^L}$, $\zeta_1^{NL}(r) = \zeta_2^{NL}(r) = A^{NL} r^{-\alpha^{NL}}$, $\Pr_1^L(r) = 1 - \frac{r}{d_1}$, and $\Pr_2^L(r) = 0$. For clarity, this 3GPP special case is referred to as **3GPP Case 1** in the sequel.

Moreover, as another application of our analytical work and to demonstrate that our conclusions have general significance, we consider another widely used LoS probability

function, which is a two-piece exponential function defined in the 3GPP as [6], [10]

$$\Pr^L(r) = \begin{cases} 1 - 5 \exp(-R_1/r), & 0 < r \leq d_1 \\ 5 \exp(-r/R_2), & r > d_1 \end{cases}, \quad (29)$$

where R_1 and R_2 are constants, and $d_1 = \frac{R_1}{\ln 10}$. The combination of the path loss function in (27) and the LoS probability function in (29) can then be deemed as a special case of the proposed path loss model in (1) with the following substitution: $N = 2$, $\zeta_1^L(r) = \zeta_2^L(r) = A^L r^{-\alpha^L}$, $\zeta_1^{NL}(r) = \zeta_2^{NL}(r) = A^{NL} r^{-\alpha^{NL}}$, $\Pr_1^L(r) = 1 - 5 \exp(-R_1/r)$, and $\Pr_2^L(r) = 5 \exp(-r/R_2)$. For clarity, this combined case with both the path loss function and the LoS probability function coming from [6] is referred to as **3GPP Case 2** hereafter.

As justified in [10], we mainly use 3GPP Case 1 to generate the numerical results in Section V, because it provides tractable results for $\{f_{R,n}^{Path}(r)\}$ and $\{\mathcal{L}_{I_{agg}}^{Path}(s)\}$ in (9)-(16) of Theorem 1. We will also use Theorem 1 to numerically investigate 3GPP Case 2, and show that similar conclusions like those for 3GPP Case 1 can also be drawn for 3GPP Case 2.

V. SIMULATION AND DISCUSSION

In this section, we investigate network performance and use numerical results to validate the accuracy of our analysis. According to Tables A.1-3, A.1-4 and A.1-7 of [6] and [7], we adopt the following parameters for 3GPP Case 1: $d_1 = 300$ m, $\alpha^L = 2.09$, $\alpha^{NL} = 3.75$, $A^L = 10^{-10.38}$, $A^{NL} = 10^{-14.54}$, $P = 24$ dBm, $P_N = -95$ dBm (including a noise figure of 9 dB at each UE). Besides, the UE density ρ is set to 100 UEs/km², 300 UEs/km² and 600 UEs/km² to represent a SCN with a low traffic load, a medium traffic load and a high traffic load, respectively [3].

To evaluate the impact of different path loss models on our conclusions, we have also investigated the results for a single-slope path loss model that does not differentiate LoS and NLoS transmissions [4]. In such path loss model, one path loss exponent α is defined, the value of which is assumed to be $\alpha = \alpha^{NL} = 3.75$. Note that in this single-slope path loss model, the density of the active BSs is assumed to be $\lambda_0(3.5)$ shown in (19) [5].

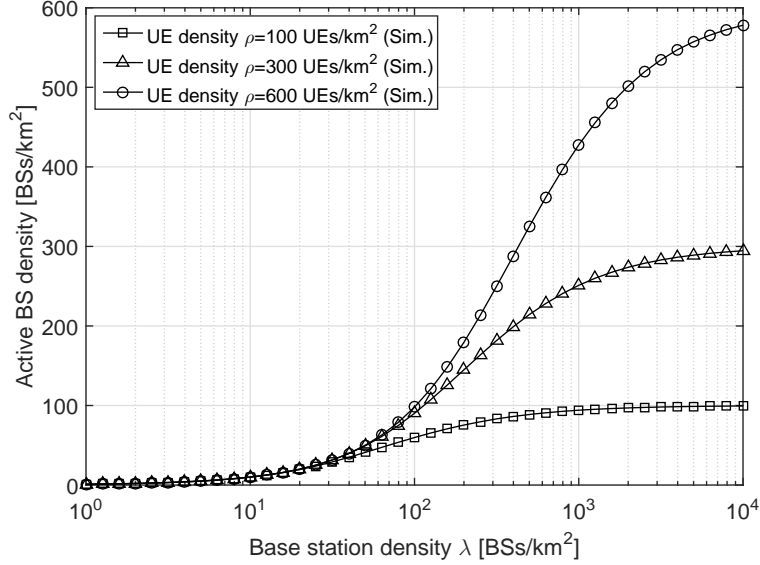


Fig. 2. The density of the active BSs with various values of ρ for 3GPP Case 1.

A. The Value of q^* for the Approximate $\tilde{\lambda}$ in 3GPP Case 1

For 3GPP Case 1, the simulated results on the density of the active BSs, i.e., $\tilde{\lambda}$, for various values of ρ are shown in Fig. 2. As can be seen from Fig. 2, more BSs will be activated with the network densification. However, the value of $\tilde{\lambda}$ caps at ρ , because one UE can activate at most one BS for its service.

Considering Proposition 4, we conduct a bisection search to numerically find the optimal q^* for the approximate $\tilde{\lambda}$. Based on the MMSE criterion proposed in Subsection IV-E, we obtain $q^* = 4.73$, $q^* = 4.18$ and $q^* = 3.97$ for the cases of $\rho = 100$ UEs/km², $\rho = 300$ UEs/km² and $\rho = 600$ UEs/km², respectively. In Figs. 3, 4 and 5, we show the average errors on the estimated number of the active BSs based on $\tilde{\lambda}^{\text{UB}}$, $\tilde{\lambda}^{\text{LB}}$, and $\lambda_0(q^*)$ for various values of ρ . Note that in those figures, all results are compared against the simulation results, which form the baseline results with zero errors. Also note that as discussed in Subsection IV-B, the exact expression of $\tilde{\lambda}^{\text{LB}}$ is still unknown up to now, but it can be well approximated by $\lambda_0(q)$ presented in (19). Hence, the results of $\lambda_0(q)$ are displayed in those figures to represent an lower bound of $\tilde{\lambda}$.

From Figs. 3, 4 and 5, we can draw the following conclusions:

- The proposed upper bound $\tilde{\lambda}^{\text{UB}}$ and lower bound $\tilde{\lambda}^{\text{LB}}$ are valid compared with the simulation results. More specifically, $\tilde{\lambda}^{\text{UB}}$ and $\tilde{\lambda}^{\text{LB}}$ are always larger (showing positive errors)

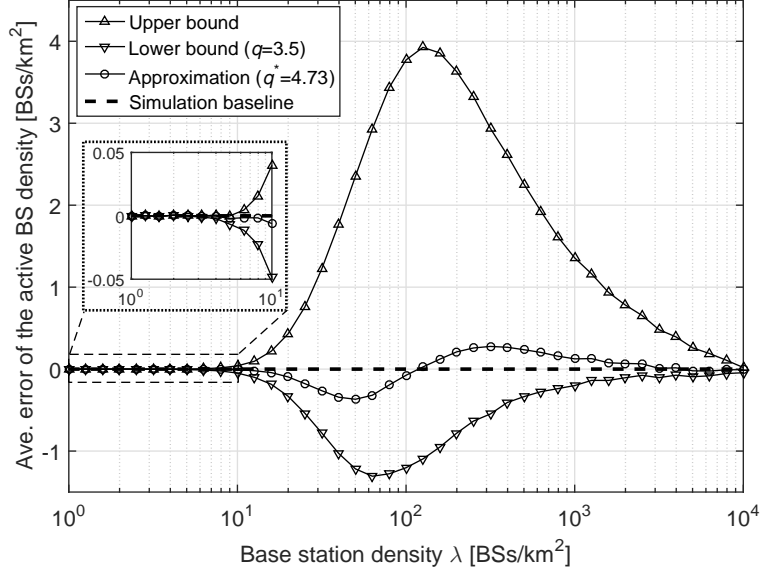


Fig. 3. The average error of the active BS density for 3GPP Case 1 ($\rho = 100$ UEs/km²).

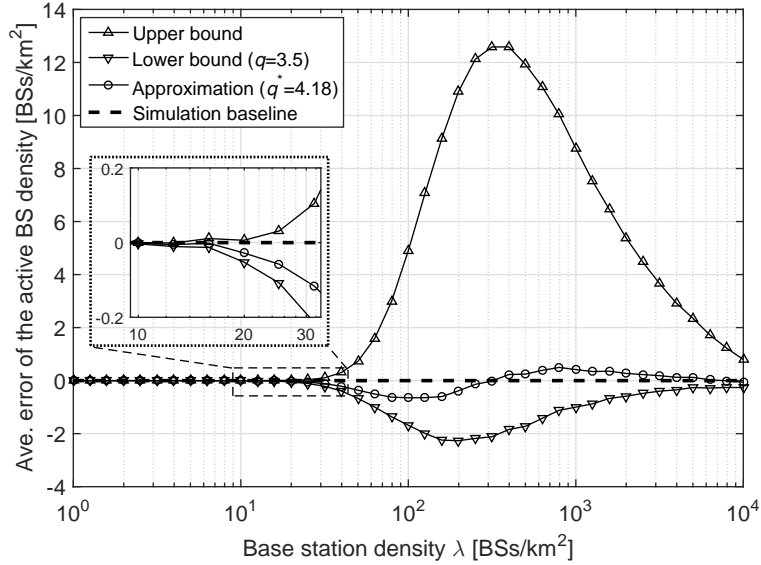


Fig. 4. Average error of the active BS density for 3GPP Case 1 ($\rho = 300$ UEs/km²).

and smaller (showing negative errors) than the simulation baseline results, respectively.

- $\tilde{\lambda}^{\text{UB}}$ is tighter than $\tilde{\lambda}^{\text{LB}}$ when λ is relatively small, e.g., when $\lambda < 30$ BSs/km² in the case of $\rho = 300$ UEs/km².
- $\tilde{\lambda}^{\text{LB}}$ is much tighter than $\tilde{\lambda}^{\text{UB}}$ for dense and ultra-dense SCNs, e.g., $\lambda > 100$ BSs/km².
- For the proposed approximation $\lambda_0(q^*)$, the value of q^* varies with ρ , which is attributable to the considered path loss model and the adopted UAS (each UE should be connected to the BS with the smallest path loss, not necessarily the closest BS). It

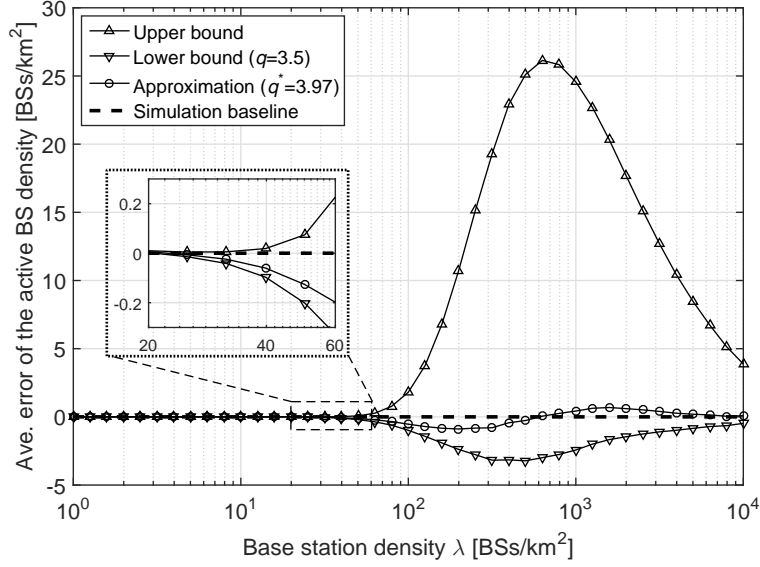


Fig. 5. Average error of the active BS density for 3GPP Case 1 ($\rho = 600$ UEs/km²).

is interesting to note that as ρ approaches infinity, q^* becomes closer to 3.5, which is derived based on the naive UAS, in which each UE is associated with its nearest BS.

- The maximum error associated with $\lambda_0(q^*)$ is smaller than those of $\tilde{\lambda}^{\text{UB}}$ and $\tilde{\lambda}^{\text{LB}}$, e.g., when $\rho = 300$ UEs/km², the maximum error resulting from $\lambda_0(q^*)$ is around ± 0.5 BSs/km², while those given by $\tilde{\lambda}^{\text{UB}}$ and $\tilde{\lambda}^{\text{LB}}$ are around 12 BSs/km² and -2 BSs/km², respectively. Hence, $\lambda_0(q^*)$ gives a better estimation on $\tilde{\lambda}$ than both $\tilde{\lambda}^{\text{UB}}$ and $\tilde{\lambda}^{\text{LB}}$.

B. Evaluation of the Accuracy of Theorem 1

In Fig. 6, we show the results of $p^{\text{cov}}(\lambda, \gamma)$ when $\rho = 300$ UEs/km² and $\gamma = 0$ dB, with $q^* = 4.18$ plugged into Proposition 4. As discussed in Section III, the total UE number in cellular networks is usually much higher the number of the active UEs, but at a certain time slot and on a certain frequency band, the active UEs with data traffic demands are not too many. A typical density of the active UEs in 5G is round $\rho = 300$ UEs/km² [3], which will thus be used to evaluate network performance in the following subsections. Note that in our numerical results here and in the following subsections, the proposed analysis is given by Theorem 1 and Proposition 4. As an important benchmark, we also display the results for $\rho = +\infty$ UEs/km² with all BSs active.

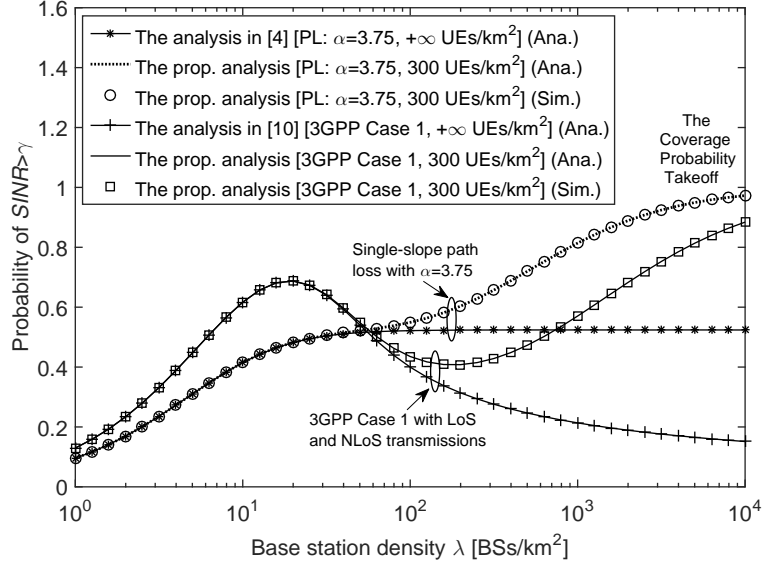


Fig. 6. The coverage probability $p^{\text{cov}}(\lambda, \gamma)$ vs. λ ($\gamma = 0$ dB, $\rho = 300$ UEs/km² and $q^* = 4.18$).

As one can observe, our analytical results given by Theorem 1 and Proposition 4 match the simulation results very well, which validate the accuracy of our analysis. In fact, Fig. 6 is essentially the same as Fig. 1, except that the results for the single-slope path loss model with $\rho = 300$ UEs/km² are also plotted here for a complete view of the performance behavior.

Moreover, Fig. 6 confirms the key observations presented in Section I:

- For the single-slope path loss model with $\rho = +\infty$ UEs/km², the coverage probability approaches a constant for dense SCNs as reported in [4]. As ρ approaches infinity, all BSs need to be active. Therefore, this scenario corresponds to a network condition that does not require the IMC, i.e., the fully loaded network.
- For 3GPP Case 1 with $\rho = +\infty$ UEs/km², the coverage probability decreases as λ increases when the network is dense enough, i.e., $\lambda > 20$ BSs/km², due to the NLoS to LoS transition of interfering paths [10], leading to a faster increase of the interference power compared with the signal power. When λ is very large, i.e., $\lambda \geq 10^3$ BSs/km², the coverage probability decreases at a slower pace because both the interference and the signal powers are LoS dominated [10].
- For both path loss models with $\rho = 300$ UEs/km², the coverage probability performance continuously increases toward one, i.e., *the Coverage Probability Takeoff*. This shows the benefits of the IMC in dense SCNs as discussed in Section I.

C. The ASE Performance

In Fig. 7, we plot the results of $A^{\text{ASE}}(\lambda, \gamma_0)$ when $\rho = 300 \text{ UEs/km}^2$ and $\gamma_0 = 0 \text{ dB}$, with $q^* = 4.18$ plugged into Proposition 4.

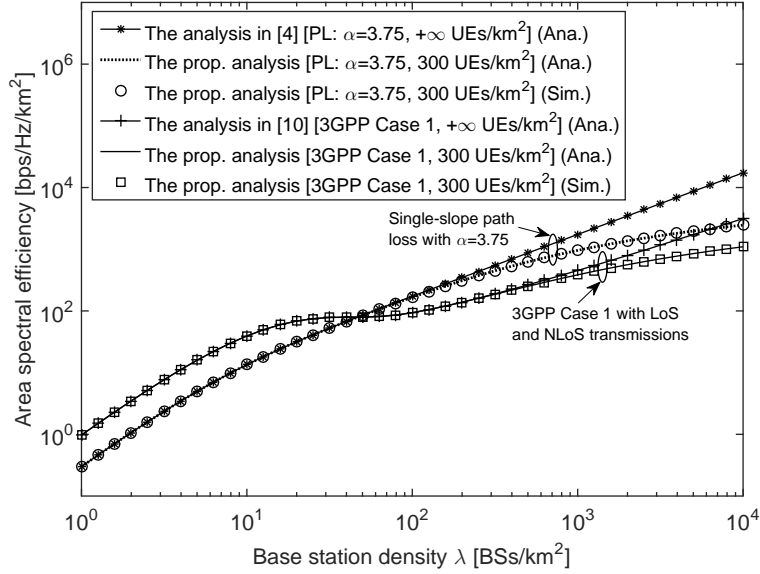


Fig. 7. The ASE $A^{\text{ASE}}(\lambda, \gamma_0)$ vs. λ ($\gamma_0 = 0 \text{ dB}$, $\rho = 300 \text{ UEs/km}^2$ and $q^* = 4.18$).

From Fig. 7, we can draw the following conclusions:

- For 3GPP Case 1, the ASE suffers from a slow growth or even a slight decrease when $\lambda \in [20, 200] \text{ BSs/km}^2$ because of the interference transition from NLoS to LoS [10]. Such performance degradation has also been confirmed in Fig. 6.
- After such BS density region of interference transition, for both path loss models with the IMC and $\rho = 300 \text{ UEs/km}^2$, the ASEs monotonically grow as λ increases in dense SCNs, but with noticeable performance gaps compared with those with $\rho = +\infty \text{ UEs/km}^2$.
- The takeaway message should not be that the IMC generates an inferior ASE in dense SCNs. Instead, as explained in Section I, since there is a finite number of the active UEs in the network, some BSs are put to sleep and thus the spatial spectrum reuse and in turn the ASE decreases. However, the per-UE performance should increase as indicated by the coverage probability performance exhibited in Fig. 6.
- It is of great interest to investigate whether the IMC can indeed improve the EE performance. This will be further studied in Subsection V-F considering practical power models with various IMC modes.

D. The Impact of α^L and Rician Fading on the ASE Performance

In Fig. 8, we investigate the performance of $A^{\text{ASE}}(\lambda, \gamma_0)$ under the assumptions of $\alpha^L = 1.09$ [10] or Rician fading [7].

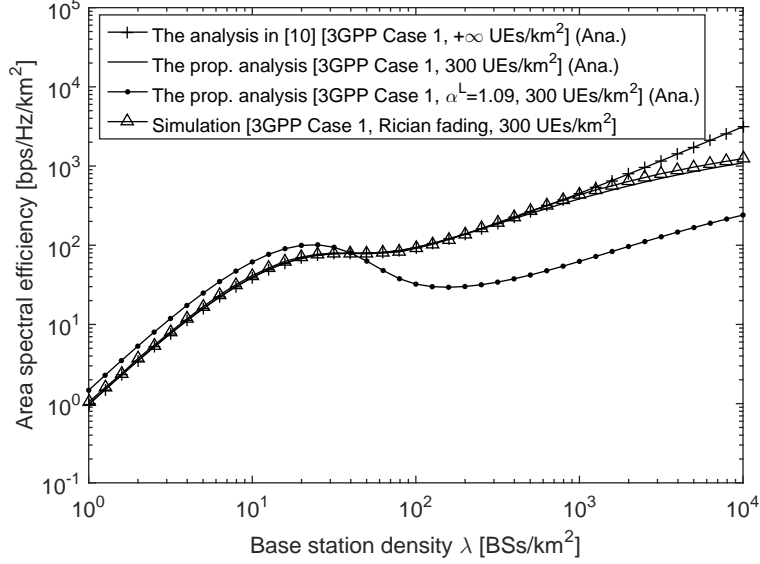


Fig. 8. The ASE $A^{\text{ASE}}(\lambda, \gamma_0)$ vs. λ with the assumptions of $\alpha^L = 1.09$ or Rician fading ($\gamma_0 = 0$ dB, $\rho = 300$ UEs/km² and $q^* = 4.18$).

Here we adopt a practical model of Rician fading in [7], where the K factor in dB scale (the ratio between the power in direct path and the power in other scattered paths) is distance dependent and it is modeled as $K[\text{dB}] = 13 - 0.03r$, where r is the distance between BS and UE in meter. Note that Theorem 1 is derived for Rayleigh fading only, and it is challenging to obtain analytical results for Rician fading. Therefore, we only display simulation results for Rician fading in Fig. 8, and leave the related theoretical analysis as our future work.

Our key conclusions from Fig. 8 are summarized as follows:

- Decreasing α^L aggravates the interference transition from NLoS to LoS, which is illustrated by an obvious ASE decrease when $\lambda \in [20, 100]$ BSs/km². This is due to the more drastic change of interference paths from NLoS to stronger LoS of $\alpha^L = 1.09$, compared with $\alpha^L = 2.09$ defined in 3GPP Case 1 [10].
- From the simulation results, we can also observe that Rician fading makes the ASE slightly better than that with Rayleigh fading, especially for a very large BS density, e.g., $\lambda > 1000$ BSs/km². The performance difference is in general very small.

- To sum up, all the conclusions in Subsection V-C are qualitatively valid for Fig. 8. Only some quantitative deviations exist.

E. The Impact of 3GPP Case 2 on the ASE Performance

In this subsection, we investigate the ASE performance for 3GPP Case 2, which has been introduced in Subsection IV-G. The parameters in the LoS probability function $\text{Pr}^L(r)$ of 3GPP Case 2 are set to $R_1 = 156$ m and $R_2 = 30$ m [6]. Here, we directly apply the numerical integration in Theorem 1 to evaluate the ASE performance for 3GPP Case 2.

First, we study the value of q^* for the approximate $\tilde{\lambda}$ in 3GPP Case 2. The simulated results on the density of the active BSs in case of various values of ρ are very similar to those shown in Fig. 2. For brevity, in Fig. 9, we only plot the average error of the density of the active BSs for $\rho = 300$ UEs/km².

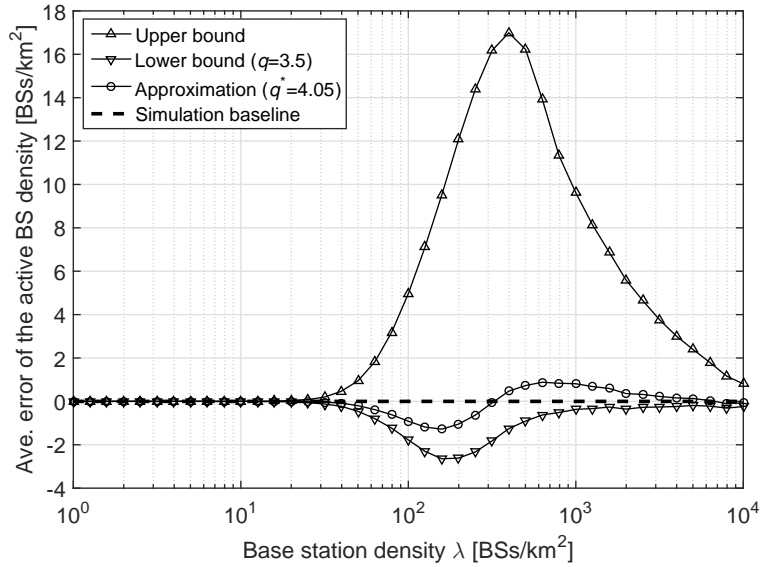


Fig. 9. Average error of the active BS density for 3GPP Case 2 ($\rho = 300$ UEs/km²).

Similar conclusions can be drawn for Fig. 9 as discussed in Subsection V-A, except for the small numerical difference of $q^* = 4.05$ for $\rho = 300$ UEs/km² in 3GPP Case 2.

In Fig. 10, we show the results of $A^{\text{ASE}}(\lambda, \gamma_0)$ for 3GPP Case 2. As one can observe, all the conclusions in Subsection V-C are qualitatively valid for Fig. 10. Only some quantitative deviations exists.

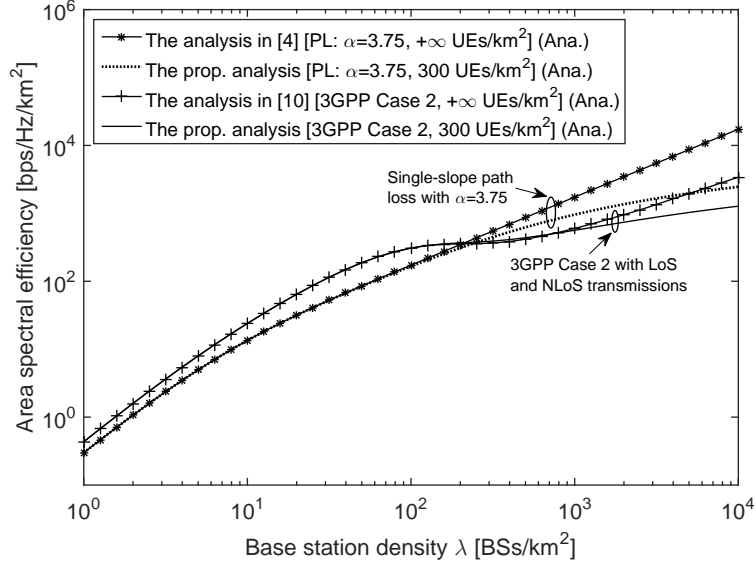


Fig. 10. The ASE $A^{\text{ASE}}(\lambda, \gamma_0)$ vs. λ with $\gamma_0 = 0$ dB for 3GPP Case 2.

F. The EE Performance

As discussed in Subsection IV-F, since we consider the realistic EE performance, we should acknowledge the fact that modern telecommunication systems usually work in the interference limited regime and the BS transmission power P should vary with λ . In this section, we formulate P using a practical power model addressed in [3]. Specifically, the transmit power of each BS is configured such that it provides a signal-to-noise-ratio (SNR) of $\eta_0 = 15$ dB at the edge of the average coverage area for the UEs with NLoS transmissions, which corresponds to the worst-case path loss. In addition, the distance from a cell-edge UE to its serving BS with an average coverage area is calculated by $r_0 = \sqrt{\frac{1}{\lambda\pi}}$, which is the radius of an equivalent disk-shaped coverage area with an area size of $\frac{1}{\lambda}$. In other words, a network with a BS density λ is now interpreted as that every unit-size area (1 km^2) can be covered by λ small cell disks, each with a radius of r_0 . Therefore, the worst-case pathloss is given by $A^{\text{NL}}r_0^{-\alpha^{\text{NL}}}$ and the required transmission power to enable a η_0 dB SNR for this case can be computed by [3]

$$P(\lambda) = \frac{10^{\frac{\eta_0}{10}} P_{\text{N}}}{A^{\text{NL}}r_0^{-\alpha^{\text{NL}}}}. \quad (30)$$

In Fig. 11, we plot the BS density dependent transmission power in dBm to illustrate this realistic power configuration when $\eta_0 = 15$ dB. Note that our modeling of P is very

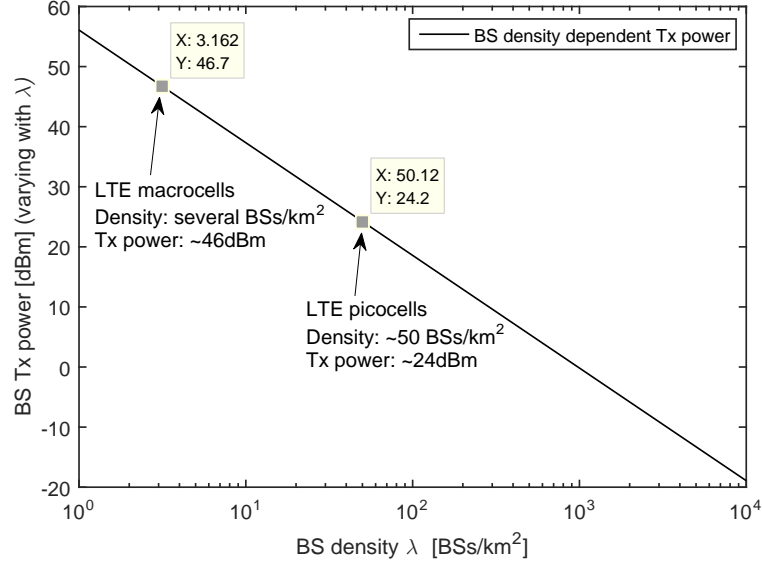


Fig. 11. The BS density dependent transmission power in dBm.

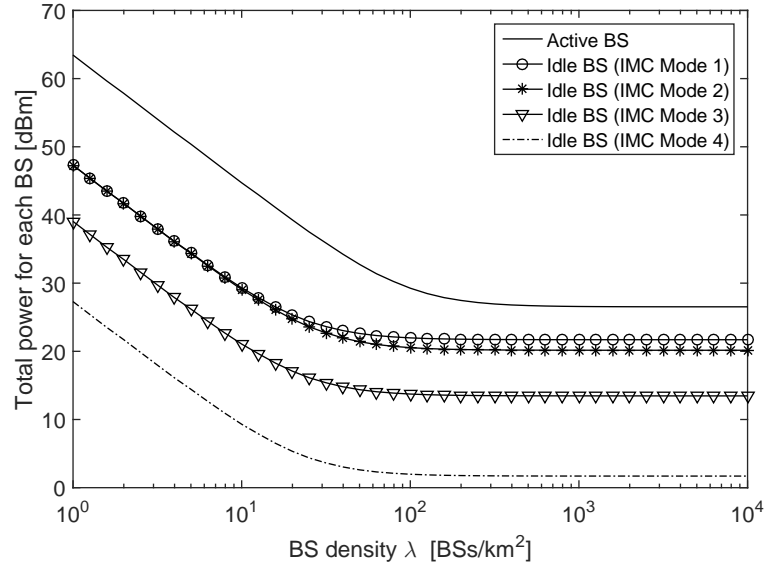


Fig. 12. The BS density dependent total power in dBm.

practical, covering the cases of macrocells and picocells recommended in the 3GPP Long-Term Evolution (LTE) networks. More specifically, the typical BS densities of LTE macrocells and picocells are respectively several BSs/km² and around 50 BSs/km² [18]. As a result, the typical P of macrocell BSs and picocells BSs are respectively assumed to be 46 dBm and 24 dBm in the 3GPP standards [18], which match well with our modeling of P in Fig. 11.

As a result of (30), $P_{\text{IMC}}^{\text{TOT}}(\lambda)$ and $P_{\text{ACT}}^{\text{TOT}}(\lambda)$ are calculated numerically using the Green-Touch power model [15] and the results are displayed in Fig. 12 assuming a future SCN

BS model in year 2020 and a 10 MHz bandwidth. From Fig. 12, we can draw the following observations:

- The total power of each active BS, i.e., $P_{\text{ACT}}^{\text{TOT}}(\lambda)$, is always larger than that of each idle BS, i.e., $P_{\text{IMC}}^{\text{TOT}}(\lambda)$, because some BS component(s) will be deactivated to save energy consumption when a BS enters an idle mode.
- As mentioned in Subsection IV-F, we consider *the Green-Touch slow idle mode* and *the Green-Touch shut-down mode* to characterize $P_{\text{IMC}}^{\text{TOT}}(\lambda)$, which are represented by IMC Mode 1 and IMC Mode 2, respectively. In comparison, IMC Mode 2 consumes less energy than IMC Mode 1 as shown in Fig. 12.
- Following [3], we also consider two futuristic idle modes to further characterize $P_{\text{IMC}}^{\text{TOT}}(\lambda)$, where their energy consumption is 15% (IMC Mode 3) or 1% (IMC Mode 4) of that of *the Green-Touch slow idle mode* (IMC Mode 1). The former mode (IMC Mode 3) accounts less energy consumption than *the Green-Touch shut-down mode* (IMC Mode 2), and the latter mode (IMC Mode 4) assumes that a BS consumes almost nothing.

Before showing the EE performance, we need to verify that our BS transmission power model shown in Fig. 11 does not heavily affect the ASE performance for dense SCNs. Otherwise, the comparison of the EE might be unfair for the interested schemes. To that end, in Fig. 13, we plot the analytical results on the ASE performance for 3GPP Case 1 when $\rho = 300 \text{ UEs/km}^2$ and $\rho = +\infty \text{ UEs/km}^2$ using the considered power models.

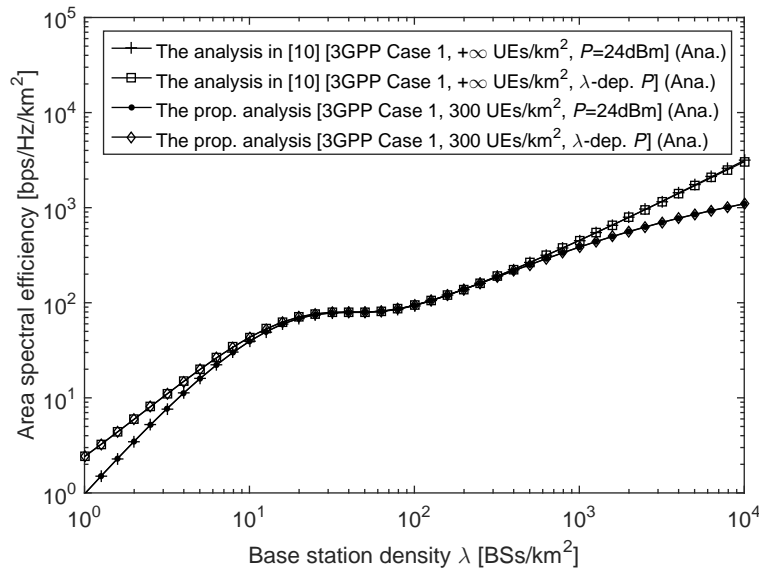


Fig. 13. The ASE performance $A^{\text{ASE}}(\lambda, \gamma_0)$ vs. λ with $\gamma_0 = 0 \text{ dB}$ and two transmission power models.

From this figure, we can draw the following conclusions:

- For both $\rho = 300 \text{ UEs/km}^2$ and $\rho = +\infty \text{ UEs/km}^2$, compared with the fixed BS transmission power of 24 dBm, the λ -dependent BS transmission power exhibited in Fig. 11 does not change the ASE performance as long as the BS density is relatively large, e.g., $\lambda > 10 \text{ BSs/km}^2$. The reason is that the considered SCN works in the interference limited regime when λ is relatively large, and in such regime, the transmit power allocated to each BS has little impact on the ASE performance, as long as all BSs in the dense SCN use the same transmission power. Thus, from the perspective of theoretical analysis on ASE for dense SCNs, both power models are equally good. However, regarding the EE performance, the λ -dependent BS transmission power should bring more power savings and be more accurate to characterize the EE performance for realistic SCNs.
- It is interesting to note that, when the BS density is relatively small (noise limited regime), e.g., $\lambda < 10 \text{ BSs/km}^2$, there is a performance gap between the ASE with the fixed BS transmission power of 24 dBm and that with the λ -dependent BS transmission power exhibited in Fig. 11. Such ASE performance gaps caused by these two power assumptions are basically the same for both cases of $\rho = 300 \text{ UEs/km}^2$ and $\rho = +\infty \text{ UEs/km}^2$. This is because when the BS density $\lambda < 10 \text{ BSs/km}^2$, almost all BSs will be activated either by a relatively large UE density of $\rho = 300 \text{ UEs/km}^2$ or by $\rho = +\infty \text{ UEs/km}^2$, which leads to the same ASE performance at a low BS density.

After confirming that the power model shown in Fig. 11 does not drastically affect the ASE performance of dense SCNs, we can now focus on the energy consumption and investigate the EE performance in a fair manner to show the benefits of the BS IMC. In Fig. 14, we plot the EE performance in the unit of bits/J for 3GPP Case 1 when $\rho = +\infty \text{ UEs/km}^2$ without IMC and $\rho = 300 \text{ UEs/km}^2$ with various IMC modes. To obtain a better visualization of the EE performance and to echo the simulation results presented in [3], we also display the EE performance using a linear scale in Fig. 15.

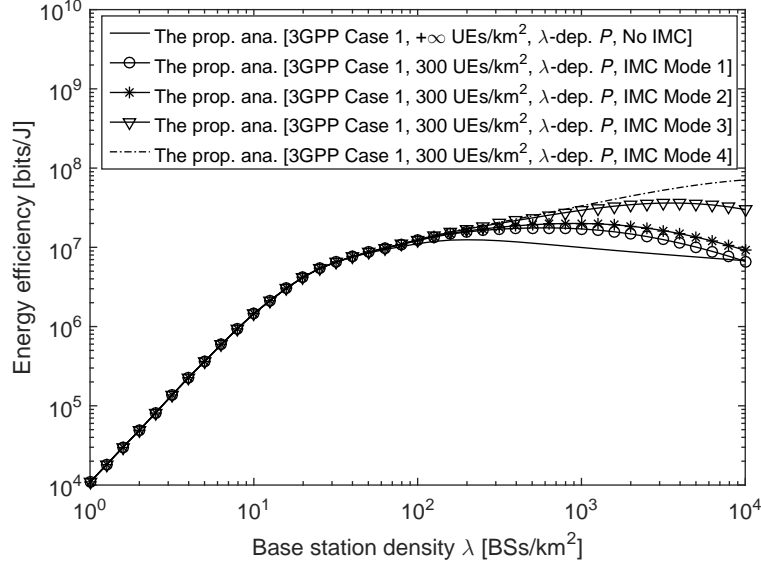


Fig. 14. The EE performance $EE(\lambda, \gamma_0)$ vs. λ with the BS density dependent P and various IMC modes (logarithm scale).

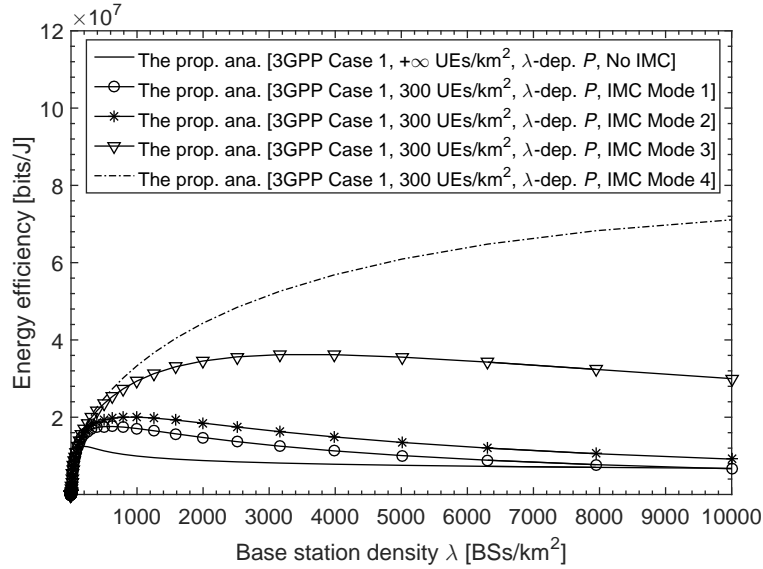


Fig. 15. The EE performance $EE(\lambda, \gamma_0)$ vs. λ with the BS density dependent P and various IMC modes (linear scale).

From Figs. 14 and 15, we can draw the following conclusions:

- As predicted in Subsection V-C, the baseline scheme with $\rho = +\infty$ UEs/km², where all BSs are active, is the least energy efficient scheme among the investigated ones, because each BS suffers from a diminishing EE return with the network densification due to the deteriorating performance of the coverage probability as the BS density increases (see Fig. 6). Such deteriorating performance is caused by the interference path transition from NLoS to LoS as discussed in previous sections.

- On the other hand, the EE performance of various IMC modes benefits from *the Coverage Probability Takeoff*, which improves the performance of each active BS as the SCN densifies, and thus the IMC scheme outperforms the baseline scheme in terms of EE. When comparing the EE performance of different IMC modes, it can be seen that the lower the power consumption in the idle mode exhibited in Fig. 12, the larger the EE of the SCN with the IMC.
- When using *the Green-Touch slow idle mode* (IMC Mode 1) and *the Green-Touch shut-down mode* (IMC Mode 2), the EE decreases with the network densification when $\lambda > 10^3$ BSs/km². This is because the increase in the ASE provided by *the Coverage Probability Takeoff* is not large enough to compensate the increase in their power consumption, mostly because idle BSs following the Green-Touch power models still consume a non-negligible amount of energy. Nevertheless, the schemes with the IMC are superior to the baseline scheme. In more detail, when $\lambda = 10^3$ BSs/km², *the Green-Touch slow idle mode* (IMC Mode 1) and *the Green-Touch shut-down mode* (IMC Mode 2) can achieve EE performance of 17.1 Mbits/J and 20.0 Mbits/J, respectively, which are around two times the EE of the baseline scheme, i.e., 9.9 Mbits/J.
- When considering the EE of the futuristic IMC Mode 3 and IMC Mode 4, the above trend starts changing. For IMC Mode 3, the EE first increases with the network densification, and then starts to decrease slowly only when λ grows very large, e.g., $\lambda > 3 \times 10^3$ BSs/km². For IMC Mode 4, idle BSs barely consume any energy, and thus the above trend significantly changes. Now the EE performance always increases with the network densification, because *the Coverage Probability Takeoff* comes into play with very little energy cost on idle BSs. As a result, when $\lambda = 10^3$ BSs/km², IMC Mode 3 and IMC Mode 4 can achieve EE performance of 29.4 Mbits/J and 33.3 Mbits/J, respectively, which triple that of the baseline scheme, i.e., 9.9 Mbits/J. Hence, schemes similar to IMC Mode 4 are needed to ensure an energy-efficient deployment of dense SCNs in 5G.

VI. CONCLUSION

In this paper, we have studied the performance impact of the IMC on dense SCNs considering probabilistic LoS and NLoS transmissions. The impact is significant, i.e., as the

BS density surpasses the UE density, the coverage probability will continuously increase toward one in dense SCNs (*the Coverage Probability Takeoff*), addressing the critical issue of coverage probability decrease caused by the NLoS to LoS transition of interference paths. Moreover, from our studies based on practical power models and path loss functions, when $\lambda = 10^3$ BSs/km², the EE performance can be doubled or even tripled using various IMC modes compared with the baseline scheme where all BSs are active. Hence, schemes similar to IMC Mode 4 are needed to ensure an energy-efficient deployment of dense SCNs in 5G networks.

APPENDIX A: PROOF OF THEOREM 1

Here we provide a straightforward and easy-to-understand proof for Theorem 1.

In (8), T_n^L and T_n^{NL} are actually the components of the coverage probability for the case when the signal comes from the n -th piece LoS path (denoted by Event B_n^L) and for the case when the signal comes from the n -th piece NLoS path (denoted by Event B_n^{NL}), respectively. In the following, we take T_n^L as an example to show the derivation. Note that the derivation of T_n^{NL} is very similar to that of T_n^L , which will thus be omitted for brevity.

To calculate T_n^L , we need to know two things so that we can perform an integral with respect to the signal-link distance r to obtain T_n^L , i.e., (i) the joint PDF of r and Event B_n^L , denoted by $f_{R,n}^L(r)$ in (9), and (ii) the coverage probability conditioned on (r, B_n^L) , i.e., $\Pr[\text{SINR} > \gamma | (r, B_n^L)]$. Note that since $f_{R,n}^{Path}(r)$ is the joint PDF of r and Event B_n^{Path} , where the string variable $Path$ takes the value of “L” and “NL” for the LoS and the NLoS cases, respectively. For convenience, $\{f_{R,n}^L(r)\}$ and $\{f_{R,n}^{NL}(r)\}$ are further stacked into piecewise functions written as

$$f_R^{Path}(r) = \begin{cases} f_{R,1}^{Path}(r), & \text{when } 0 \leq r \leq d_1 \\ f_{R,2}^{Path}(r), & \text{when } d_1 < r \leq d_2 \\ \vdots & \vdots \\ f_{R,N}^{Path}(r), & \text{when } r > d_{N-1} \end{cases}. \quad (31)$$

Furthermore, we define the cumulative distribution function (CDF) of $f_R^{Path}(r)$ as

$$F_R^{Path}(r) = \int_0^r f_R^{Path}(u) du, \quad (32)$$

and we have $F_R^L(+\infty) + F_R^{NL}(+\infty) = 1$.

By definition, $f_{R,n}^L(r)$ should be calculated as $f_{R,n|B_n^L}(r|B_n^L) \Pr[B_n^L]$, where $\Pr[B_n^L] = \Pr_n^L(r)$ from (2) and $f_{R,n|B_n^L}(r|B_n^L)$ should characterize the joint event of the following three independent sub-events:

- 1) For the typical UE, its serving BS b_o is positioned at the distance r from it and the corresponding unconditional PDF of r is $2\pi r\lambda$ [4].
- 2) There is no LoS BS that can provide a better link to the typical UE than the LoS BS b_o , the probability of which is $\exp(-\int_0^r \Pr^L(u) 2\pi u \lambda du)$ [10].
- 3) There is no NLoS BS that can provide a better link to the typical UE than the LoS BS b_o , the probability of which is $\exp(-\int_0^{r_1} (1 - \Pr^L(u)) 2\pi u \lambda du)$ [10], where r_1 is computed by (11) to find the distance at which a NLoS BS has the same signal reception level as the LoS BS b_o .

Similar to [10], it is easy to show that $f_{R,n|B_n^L}(r|B_n^L)$ should be calculated by the product of the three terms presented in the above bulletins, and thus $f_{R,n}^L(r)$ can be written as (9).

Regarding $\Pr[\text{SINR} > \gamma | (r, B_n^L)]$, it can be evaluated using the similar technique in [10] with the consideration of the density of the active BSs, i.e., $\tilde{\lambda}$, and the result has been shown in (13), where $\exp(-\frac{\gamma P_N}{P_{\zeta_n^L(r)}})$ is the probability that *the signal power exceeds the noise power* by a factor of at least γ , and $\mathcal{L}_{I_{agg}}^L(\frac{\gamma}{P_{\zeta_n^L(r)}})$ is the probability that *the signal power exceeds the aggregate interference power* by a factor of at least γ .

Considering the assumption that h follows an exponential distribution, we can invoke $\Pr[h > \gamma(a+b)] = \Pr[h > \gamma a] \Pr[h > \gamma b]$, $(a, b \in \mathbb{R}^+)$, and thus the product of the two probabilities in the above bulletins yields the probability that *the signal power exceeds the sum power of the noise and the aggregate interference* by a factor of at least γ .

Finally, by definition, T_n^L should be computed by an integral of the product of (9) and (13) over the range of $r \in (d_{n-1}, d_n]$, which concludes our proof.

APPENDIX B: PROOF OF THEOREM 2

For clarity, the main idea of our proof is summarized as follows:

- First, we derive an conditional probability that an arbitrary UE w is *not* associated with an arbitrary BS b conditioned on the distance between UE w and BS b being r . Such conditional probability is denoted by $\Pr[w \approx b | r]$.
- Next, we derive an unconditional probability that an arbitrary UE w is *not* associated with an arbitrary BS b by performing an integral over r considering the uniform distribution of UEs in the considered network. Such unconditional probability is denoted by $\Pr[w \approx b]$.
- Finally, we derive a lower bound of the probability that every UE is *not* associated with an arbitrary BS b , so that BS b should switch off its transmission. The lower bound of the BS deactivation probability is then translated to an upper bound of the density of the active BSs, i.e., $\tilde{\lambda}$.

First, according to Appendix A and the definition of $F_R^L(r)$ and $F_R^{NL}(r)$ in (32), $\Pr[w \approx b | r]$ can be calculated by (23) because $\Pr[w \approx b | r]$ should be the sum of the probabilities of the following two events that lead to the event $[w \approx b | r]$, i.e., (a) The first term of (23): The link between UE w and BS b is a LoS one with a probability of $\Pr^L(r)$ while UE w is associated with another LoS/NLoS BS that is stronger than BS b with a probability of $[F_R^L(r) + F_R^{NL}(r_1)]$, with $F_R^L(r)$ and $F_R^{NL}(r_1)$ corresponding to the cases of a stronger LoS BS and a stronger NLoS BS, respectively; and (b) The second term of (23): The link between UE w and BS b is a NLoS one with a probability of $[1 - \Pr^L(r)]$ while UE w is associated with another LoS/NLoS BS that is stronger than BS b with a probability of $[F_R^L(r_2) + F_R^{NL}(r)]$, with $F_R^L(r_2)$ and $F_R^{NL}(r)$ corresponding to the cases of a stronger LoS BS and a stronger NLoS BS, respectively.

Next, for an arbitrary BS b , we suppose that all its candidate UEs are randomly distributed in a disk Ω centered on BS b with a radius of $r_{\max} > 0$. Then, for an arbitrary UE w inside the disk Ω , $\Pr[w \approx b]$ can be computed by (22), where $\frac{2r}{r_{\max}^2}$ is the distribution density function with respect to r for UE w [4], because UEs are assumed to be uniformly distributed in the considered SCN.

Finally, the number of candidate UEs inside disk Ω , denoted by K , should follow a Poisson distribution with a parameter of $\lambda_\Omega = \rho\pi r_{\max}^2$. Thus, the probability mass function (PMF) of K can be written as [19]

$$f_K(k) = \frac{\lambda_\Omega^k e^{-\lambda_\Omega}}{k!}, \quad k \in \{0, 1, 2, \dots\}. \quad (33)$$

Hence, the probability that BS b should be muted, i.e., no UE is associated with BS b , can be computed by (21).

It is very important to note that (21) ignores the correlation between nearby UEs inside disk Ω , i.e., a UE k *not* associated with BS b may imply that a nearby UE k' should have a large probability *not* to connect with BS b , due to the possible existence of a strong BS near UEs k and k' . Therefore, Q^{off} under-estimates the probability that BS b should be muted, and thus the density of the active BSs $\tilde{\lambda}$ can be upper-bounded by $\lambda(1 - Q^{\text{off}})$, which concludes our proof.

APPENDIX C: PROOF OF THEOREM 3

The key to the proof of Theorem 3 is to show that

$$F_R(r) \leq F_R^{\text{minDis}}(r), \quad (34)$$

where $F_R(r) = F_R^{\text{L}}(r) + F_R^{\text{NL}}(r)$ is the CDF of the UE association distance under the presented UAS, with $F_R^{\text{L}}(r)$ and $F_R^{\text{NL}}(r)$ defined in (32), and $F_R^{\text{minDis}}(r)$ is the CDF of the UE association distance under the nearest-BS UAS. Note that according to [4], $F_R^{\text{minDis}}(r)$ can be written as $F_R^{\text{minDis}}(r) = 1 - \exp(-\pi\lambda r^2)$. The tedious mathematical steps to obtain (34) are relegated to the journal version of this work.

Then, based on the property of the expected value of a non-negative RV R [20], i.e., $E(R) = \int_0^{+\infty} [1 - F_R(r)] dr$, we can draw the conclusion that the expected UE association distance under the presented UAS is no smaller than that under the nearest-BS UAS, i.e., $E(R) \geq E^{\text{minDis}}(R)$. Consequently, the effective coverage area of each BS, and thus the activation probability of each BS under the presented UAS are no smaller than those under the nearest-BS UAS. Therefore, we have $\tilde{\lambda} \geq \tilde{\lambda}^{\text{minDis}}$, which completes our proof.

REFERENCES

- [1] CISCO, “Cisco visual networking index: Global mobile data traffic forecast update (2013-2018),” Feb. 2014.
- [2] 3GPP, “TR 36.872: Small cell enhancements for E-UTRA and E-UTRAN - Physical layer aspects,” Dec. 2013.
- [3] D. López-Pérez, M. Ding, H. Claussen, and A. Jafari, “Towards 1 Gbps/UE in cellular systems: Understanding ultra-dense small cell deployments,” *IEEE Communications Surveys Tutorials*, vol. 17, no. 4, pp. 2078–2101, Jun. 2015.
- [4] J. Andrews, F. Baccelli, and R. Ganti, “A tractable approach to coverage and rate in cellular networks,” *IEEE Transactions on Communications*, vol. 59, no. 11, pp. 3122–3134, Nov. 2011.
- [5] S. Lee and K. Huang, “Coverage and economy of cellular networks with many base stations,” *IEEE Communications Letters*, vol. 16, no. 7, pp. 1038–1040, Jul. 2012.
- [6] 3GPP, “TR 36.828: Further enhancements to LTE Time Division Duplex (TDD) for Downlink-Uplink (DL-UL) interference management and traffic adaptation,” Jun. 2012.
- [7] Spatial Channel Model AHG, “Subsection 3.5.3, Spatial Channel Model Text Description V6.0,” Apr. 2003.
- [8] X. Zhang and J. Andrews, “Downlink cellular network analysis with multi-slope path loss models,” *IEEE Transactions on Communications*, vol. 63, no. 5, pp. 1881–1894, May 2015.
- [9] T. Bai and R. Heath, “Coverage and rate analysis for millimeter-wave cellular networks,” *IEEE Transactions on Wireless Communications*, vol. 14, no. 2, pp. 1100–1114, Feb. 2015.
- [10] M. Ding, P. Wang, D. López-Pérez, G. Mao, and Z. Lin, “Performance impact of LoS and NLoS transmissions in dense cellular networks,” *IEEE Transactions on Wireless Communications*, vol. 15, no. 3, pp. 2365–2380, Mar. 2016.
- [11] M. Ding, D. López-Pérez, G. Mao, P. Wang, and Z. Lin, “Will the area spectral efficiency monotonically grow as small cells go dense?” *IEEE GLOBECOM 2015*, pp. 1–7, Dec. 2015.
- [12] Z. Luo, M. Ding, and H. Luo, “Dynamic small cell on/off scheduling using stackelberg game,” *IEEE Communications Letters*, vol. 18, no. 9, pp. 1615–1618, Sept 2014.
- [13] C. Li, J. Zhang, and K. Letaief, “Throughput and energy efficiency analysis of small cell networks with multi-antenna base stations,” *IEEE Transactions on Wireless Communications*, vol. 13, no. 5, pp. 2505–2517, May 2014.
- [14] T. Zhang, J. Zhao, L. An, and D. Liu, “Energy efficiency of base station deployment in ultra dense hetnets: A stochastic geometry analysis,” *IEEE Wireless Communications Letters*, vol. 5, no. 2, pp. 184–187, Apr. 2016.
- [15] B. D. Claude Desset and F. Louagie, “Flexible Power Model of Future Base Stations: System Architecture Breakdown and Parameters,” Green Touch.
- [16] S. Singh, H. Dhillon, and J. Andrews, “Offloading in heterogeneous networks: Modeling, analysis, and design insights,” *IEEE Transactions on Wireless Communications*, vol. 12, no. 5, pp. 2484–2497, May 2013.
- [17] R. L. Burden and J. D. Faires, *Numerical Analysis (3rd Ed.)*. PWS Publishers, 1985.
- [18] 3GPP, “TR 36.814: Further advancements for E-UTRA physical layer aspects (Release 9),” Mar. 2010.
- [19] J. G. Proakis, *Digital Communications (4th Ed.)*. New York: McGraw-Hill, 2000.
- [20] A. Papoulis, *Probability, Random Variables, and Stochastic Processes*. New York: McGraw-Hill, 1984.